Title	Optically pumped whispering-gallery mode lasing from 2-micron GaN micro-disks pivoted on Si
Author(s)	Zhang, Y; Ma, Z; Zhang, X; Wang, T; Choi, HW
Citation	Applied Physics Letters, 2014, v. 104 n. 22, article no. 221106, p. 221106-1-221106-4
Issued Date	2014
URL	http://hdl.handle.net/10722/202849
Rights	Applied Physics Letters. Copyright © American Institute of Physics.

AIP | Applied Physics Letters

Optically pumped whispering-gallery mode lasing from 2-μm GaN micro-disks pivoted on Si

Yiyun Zhang, Zetao Ma, Xuhui Zhang, T. Wang, and H. W. Choi

Citation: Applied Physics Letters **104**, 221106 (2014); doi: 10.1063/1.4881183
View online: http://dx.doi.org/10.1063/1.4881183
View Table of Contents: http://scitation.aip.org/content/aip/journal/apl/104/22?ver=pdfcov
Published by the AIP Publishing

Optically pumped whispering-gallery mode lasing from 2-μm GaN micro-disks pivoted on Si

Yiyun Zhang,[1] Zetao Ma,[1] Xuhui Zhang,[1] T. Wang,[2] and H. W. Choi[1,a)]
[1]*Department of Electrical and Electronic Engineering, The University of Hong Kong, Pokfulam Road, Hong Kong*
[2]*Department of Electronic and Electrical Engineering, University of Sheffield, Mappin Street, Sheffield S1 3JD, United Kingdom*

(Received 4 December 2013; accepted 19 May 2014; published online 3 June 2014)

2-μm micro-disks containing InGaN/GaN quantum wells supported on a tiny Si nanotip are fabricated via microsphere lithography followed by dry and wet etch processes. The micro-disks are studied by photoluminescence at both room-temperature and 10 K. Optically pumped blue lasing at room-temperature is observed via whispering-gallery modes (WGMs) with a lasing threshold as low as 8.43 mJ/cm^2. Optical resonances in the micro-disks are studied through numerical computations and finite-difference time-domain simulations. The WGMs are further confirmed through the measured broadband transmission spectrum, whose transmission minima coincide well with predicted WGM frequencies. © *2014 AIP Publishing LLC*. [http://dx.doi.org/10.1063/1.4881183]

Optical cavities are integral building blocks of semiconductor lasers. With growing emphasis on high-density monolithic integration of photonic components, demands on the qualities of optical cavities become increasingly stringent, as are processes associated with their fabrication.[1] Designs for optical cavities have also diversified from rectangular slabs to complex structures such as photonic crystals,[2] micro-disks,[3] nano-wires,[4] and nanopillars,[5] with the target of achieving high-quality lasing. Advances of the III-nitride material system has opened up new opportunities for the development of laser diodes that emit at short wavelengths without frequency up-conversion, avoiding hefty conversion losses. GaN-based micro-disk lasers, in particular, have drawn much interest owing to their wide wavelength coverage from ultraviolet to visible, high optical gains benefitting from InGaN/GaN multiple quantum wells (MQWs), small model volumes as well as simple architectures without the need for mirrors, making them well-positioned for monolithic integration.[6] The fact that III-nitrides are typically grown on sapphire substrates poses significant challenges in the formation of micro-disk cavities; nevertheless such obstacle has been overcome through photoelectrochemical etching[7–9] and wet chemical etching[10,11] amongst others. Apart from these methods, we have demonstrated the pivoted GaN micro-disk structure using GaN-on-Si as starting materials. After photolithographic patterning and dry etch formation of 20-μm micro-disks, the GaN disks are partially released from their Si substrates through wet etching, leaving behind tiny pivots as mechanical supports.[12] Being on a Si platform provides the additional possibility of integration with increasingly popular Si-based photonic components.[13–15] However, those reported micro-disks, being in the early stages of development, exhibited mediocre optical characteristics, including having large modal volumes giving rise to multi-mode photo-pumped lasing; rough, and non-vertical facets resulting in low quality factors of ~80; most importantly, the InGaN/GaN quantum wells (MQWs) within the micro-disk were not efficient enough to support lasing at visible light range nor at room temperature. Overcoming these limitations calls for micro-disks with smooth and vertical sidewalls as well as a reduction of disk dimensions. In this work, an optimized version of the pivoted GaN-on-Si micro-disk is demonstrated, riding on advances in GaN-on-Si material quality and micro-fabrication processes. Microsphere lithography replaces photolithography to produce pivoted GaN micro-disks on Si substrate with reduced dimensions and smooth facets, leading to the demonstration of optically pumped room-temperature (RT) lasing via Whispering-gallery modes (WGMs).

The micro-disks are fabricated on wafers grown on two-inch (111) silicon substrate with a 150 nm high-temperature AlN buffer grown at 1195 °C, a 500 nm GaN layer grown at 1125 °C, 5 periods of InGaN/GaN (2.5 nm/10 nm) MQWs, topped with a 10 nm GaN cladding layer grown at 880 °C. The InGaN wells and the GaN barriers were grown at 800 °C and 880 °C, respectively. The diagrams in Fig. 1 illustrate the

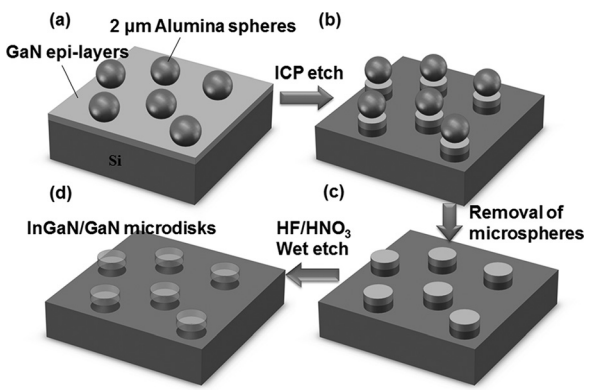

FIG. 1. Schematic diagrams of fabrication process flow for InGaN/GaN micro-disks on Si: (a) spin-coating of sparsely distributed Alumina microspheres, (b) ICP dry etch, (c) removal of microspheres followed by HF/HNO_3 wet etch for 1 min, and (d) DI water cleaning to remove residues.

a)Author to whom correspondence should be addressed. Electronic mail: hwchoi@hku.hk. Tel.: (852) 28592693. Fax: (852) 25598738.

process flow for the micro-disks. Alumina (Al_2O_3) spheres with nominal diameters of 2 μm are initially dispersed in de-ionized (DI) water at a low volume ratio of 1:100. 5 μL of the suspension is pipetted onto the surface on the GaN/Si wafer, which is then spin-coated at 300 rpm. Such coating conditions ensure that the spheres are not packed together. The choice of hard alumina instead of commonly used silica ensures sufficient etch selectivities so that the spheres maintain their sphericities and dimensions throughout the etch. The wafer is then over-etched for 2 min using Ar/Cl_2 gases (10 sccm/15 sccm) by inductively coupled plasma (ICP) etching to form sparsely distributed micro-pillars. The etch parameters were 450 W of coil power and 135 W of platen power under a chamber pressure of 5 mTorr. The nitride materials not covered with microspheres must be completely removed to expose the Si substrate, as illustrated in Fig. 1(b). Residual Al_2O_3 microspheres sitting on top of the micro-pillars are then removed by sonification in DI water. The wafer is then immersed into an HF/HNO_3 (1:1) solution which etches the Si base beneath the GaN micro-disks, creating undercuts. In this step, the wet-etch duration has to be precisely controlled so as to retain a tiny Si nanotip to support the upper GaN micro-disk, whilst minimizing the GaN-Si interface for maximum optical confinement.

The field-emission scanning electronic microscope (FE-SEM) image in Fig. 2(a) shows a single ~2 μm Al_2O_3 sphere on the GaN/Si wafer after ICP etching. From Fig. 2(a), the etch depth is determined to be ~1.2 μm, or ~400 nm beyond the 800-nm-thick GaN epi-layers; the 400-nm-thick Si base underneath the GaN micro-disks facilitate lateral etching during the wet-etch process for creating an undercut. A magnified view of the sidewall, as shown in Fig. 2(b), reveals striations along the vertical direction on the otherwise smooth sidewall surface. Such striations tend to terminate at the locations of V-shape pits (V-pits) at the top surface. When the boundary of a micro-disk coincides with the site of a V-pit, the threading dislocation connected to the V-pit becomes exposed along the sidewall, which enlarges during plasma etching due to preferential etching[16] to form striations. Since the sidewall roughness is an important factor affecting the quality of a microcavity,[8] a reduction of V-pit density through optimization of the low-temperature growth of InGaN QWs will not only improve the quantum efficiency but also improve sidewall smoothness. An oblique view of a freestanding GaN micro-disk pivoted on Si is shown in Fig. 2(c). After wet-etching, the bottom AlN surface will be exposed to promote light confinement within the micro-disk at the AlN-air interface, forming a Fabry-Perot cavity in the vertical direction with the upper GaN-air interface.[15] As observed from Fig. 2(c), the micro-disks possess near-90° vertical sidewalls, as well as excellent circularity, ensuring that light emitted from the MQWs can be efficiently coupled to WG modes. Furthermore, the sidewall becomes somewhat smoother after the wet-etch process, especially at the near-surface region, evident from the SEM image in Fig. 2(d).

The photoluminescence (PL) measurements are conducted at 10 K and RT of ~300 K using a diode-pumped solid-state (DPSS) 349 nm, 4 ns, and 1 kHz pulsed laser (Spectra Physics Explorer) as an excitation source. The PL signals are probed with an optical fiber coupled into the 10 μm entrance slit of a 500 mm spectrograph (Acton SP2500), dispersed by a 2400 l/mm grating to a cooled charged-coupled device (CCD)(Princeton Instrument PIXIS), offering optical resolutions of 0.04 nm. The fiber probe is placed in proximity to the micro-disk at an angle of ~10° to the horizontal plane. Fig. 3(a) plots room-

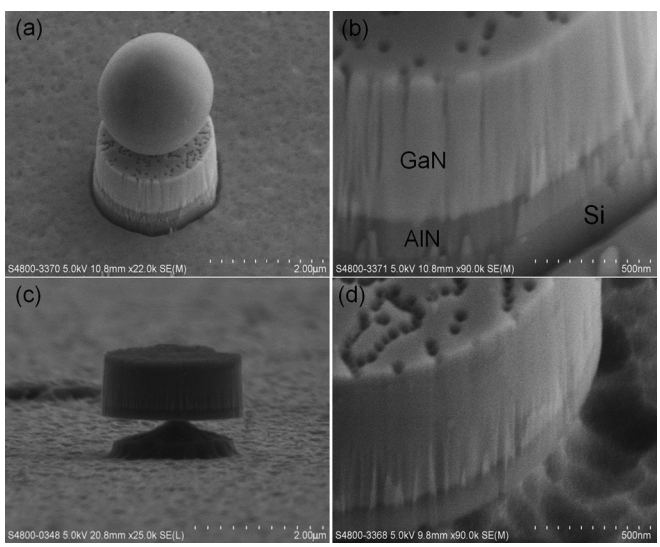

FIG. 2. (a) A single alumina sphere of ~2 μm in diameter on top of a micro-pillar after ICP etching. (b) Close-up view of the GaN/Si micro-pillar sidewall after ICP dry etch. (c) An InGaN/GaN micro-disk pivoted on Si and (d) close-view of the pivoted micro-disk.

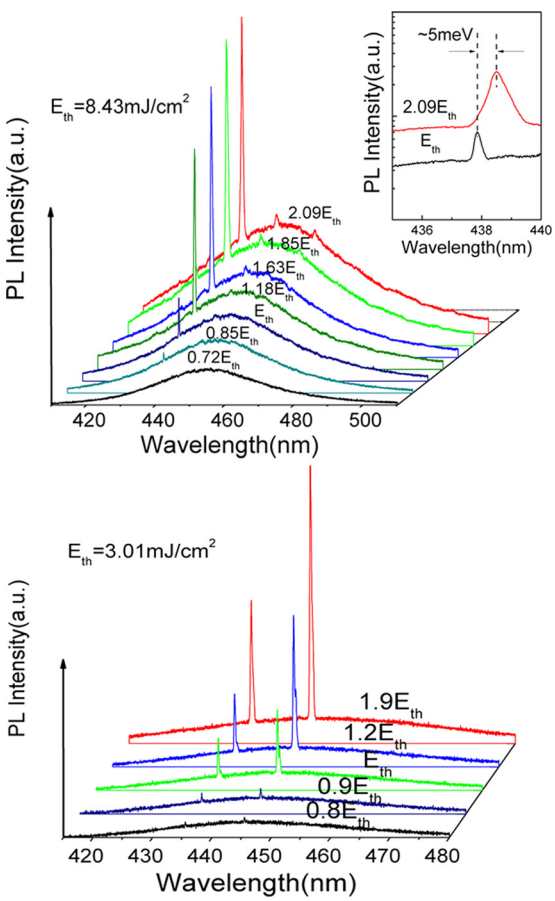

FIG. 3. Excitation-energy-dependent PL spectra of the micro-disks at (a) room-temperature and (b) 10 K. The spectra have been offset vertically for clarity. The plot in the inset shows red-shift of the WGM wavelength as excitation is raised from E_{th} to $2.09E_{th}$.

temperature PL spectra of a micro-disk at varying excitation energy densities. The spectra have been offset vertically for clarity. When the excitation exceeds the threshold value of 8.43 mJ/cm^2 (E_{th}), a sharp spectral feature emerges at a center wavelength of ~437.8 nm. As the excitation is raised further, additional resonant modes emerge gradually across the spectrum. The corresponding excitation-energy-dependent PL spectra at 10 K are presented in Fig. 3(b). At 10 K, two distinct lasing peaks can be observed at 435.5 nm and 445.4 nm, respectively. The wavelength-shift of the WGM from 437.8 to 435.5 nm results from the change in refraction index between 10 K and RT. The lasing threshold is decreased to 3.01 mJ/cm^2 at cryogenic temperatures as the MQWs become more efficient when non-radiative recombination is mostly inhibited. With increasing excitation nonlinear increases in integrated PL intensities of the WGM can be observed beyond the threshold at both 10 K and RT, as plotted in Fig. 4(a); such nonlinear increases are characteristic of stimulated emission. Based on these *S*-shaped curves, the spontaneous emission coupling factors at 10 K and RT can be estimated to be $\beta \approx \sim 0.14$ and ~0.11, respectively, taking the ratio of PL intensities below and above the threshold. The Purcell factor (F_p) is further evaluated according to the relation $F_p = \beta/(1-\beta)$, from which a value of $F_p \approx \sim 0.16$ and ~0.12 can be obtained at 10 K and RT, respectively. Since $F_p \propto Q/V$, further improvement of the Purcell factor calls for smaller and thinner cavities with an even lower mode volume (V) to suppress the number of optical modes within the cavity. Fig. 4(b) plots the line-width evolution of the WGM at 437.8 nm as a function of excitation energy density at 10 K and RT, respectively. At 10 K, the spectral line-width narrows from ~0.89 nm to ~0.29 nm as the excitation raises from 2.05 to 3.01 mJ/cm^2, while the line-width narrows from ~1.07 nm to ~0.31 nm at RT as the excitation approaches threshold (E_{th}). Spectral narrowing is a manifestation of increased temporal coherence of emission in the lasing regime,[9] where selective amplification of one frequency occurs as a result of positive feedback. Above the threshold, the WGM line-width mildly broadens, attributed to free carrier absorption under high excitation.[15] Meanwhile, a red-shift of the WGM from ~437.8 nm towards ~438.5 nm at RT can be observed as the excitation increases from E_{th} to ~2.09E_{th}, as shown in the inset of Fig. 3(a), which suggests that the micro-disk cavity is suffering from heating effects, being mounted on a tiny Si post. The electron-hole plasma (EHP) effect may also be a contributing factor.[4] The inset of Fig. 4(b) shows CCD-captured optical images of a single microdisk pumped below and above the lasing threshold. Above threshold, a periodical pattern along the micro-disk boundary as well as bright speckles within the micro-disk can be observed, both of which are signs of coherent light emission.[11]

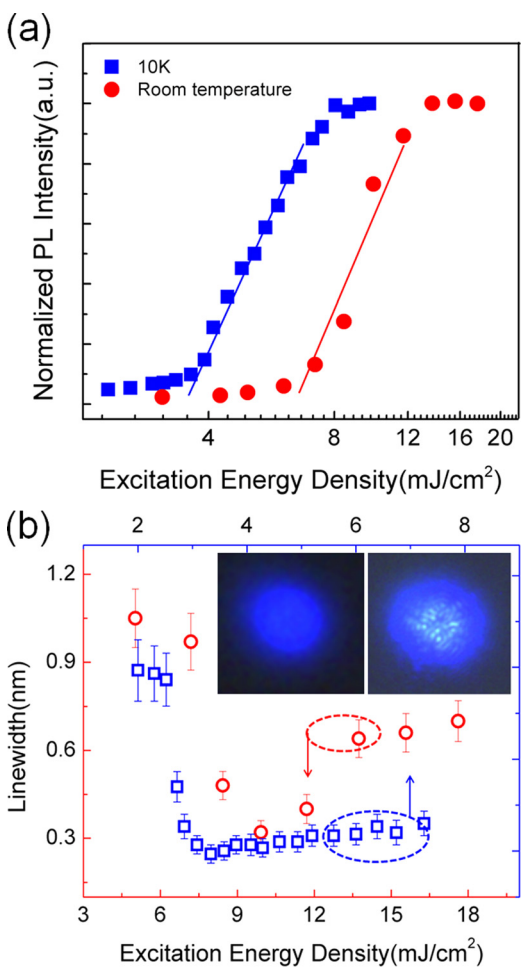

FIG. 4. (a) Normalized PL intensities of the spectral peak centered at ~437.8 nm with increasing excitation energy densities at 10 K and at room temperature. (b) Spectral line-widths for the WGMs at ~437.8 nm as a function of excitation energy density at 10 K and at room temperature. 7 μm × 7 μm CCD-captured optical images of a single microdisk pumped below and above the lasing threshold are shown in its inset.

Besides the dominant lasing mode, additional WGMs can be observed from the PL spectra at higher excitations at room temperature. The PL spectrum at the excitation condition of ~2.09E_{th} is re-plotted in Fig. 5(a). To identify these peaks, the WGM wavelengths and free spectral range (*FSR*) within the micro-disk cavity are further analyzed through numerical computations and finite-difference time-domain (FDTD) simulations. By solving the two-dimensional (2D) Helmholtz equation in cylindrical coordinate via separation of variables (omitting the coordinate dependence of the EM field in the z direction) and applying the boundary conditions for a micro-disk geometry, the following Eigen function is obtained:[17]

$$J_m(kn_{eff}a)H'_m(ka) - \beta J'_m(kn_{eff}a)H_m(ka) = 0, \qquad (1)$$

where a is the micro-disk radius, $\beta = n_{eff}$ for TM ($H_z = 0$) mode, and $\beta = 1/n_{eff}$ for TE ($E_z = 0$) mode, respectively. Here, J_m and H_m are the Bessel and Hankel functions of the first kind, m the azimuthal modal index, the constant $C_m = J_m(kn_{eff}a)/H_m(ka)$, and n_{eff} the effective refractive index of the micro-disk ($n_{eff} = \sim 2.5$). A good agreement with the experimentally measured WGM wavelengths and *FSR* can be found for a radius a of ~1.12 μm, which is slightly larger than the nominal diameters of microspheres, attributed to the non-uniformity of the Al_2O_3 microspheres (±10%). According to the numerical calculations, all the spectral peaks belong to second-order mode family ($n = 2$) of different mode numbers ($m = 32, \ldots, 26$), where n and m represent the mode numbers in the radial and azimuthal direction, respectively, as labeled on the spectral plot of Fig. 5(a). The

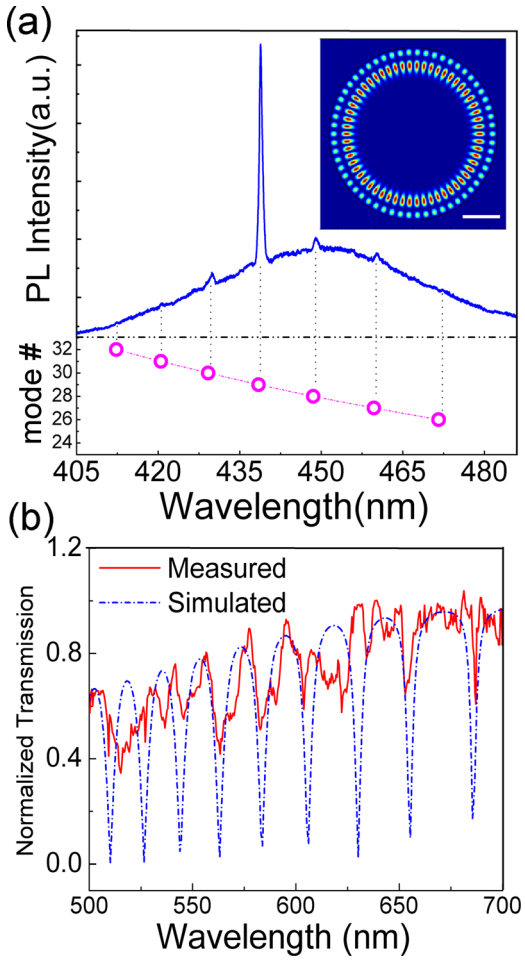

FIG. 5. (a) PL spectra from the micro-disk at the excitation condition of $\sim 2.09E_{th}$ and the mode numbers identified by numerical calculations. The FDTD simulated pattern for second-order WGMs at ~438.5 nm is shown in the inset. Regions shaded in red and blue represent the highest and lowest field intensities respectively. The micro-disk boundary is defined by the black line, while the scale bar is 500 nm long. (b) Normalized transmission spectrum measured from the InGaN/GaN micro-disks, together with the FDTD simulated transmission plot.

fundamental order mode family ($n = 1$) is not detectable, as these are lossy resonant modes with electric fields concentrated near the micro-disk boundary.[8] These calculated results are also consistent with 2D-FDTD simulations carried out over the entire emission band. Herein the simulation, the radius of the micro-disk cavity and the effective refractive index of GaN are set to be 1.12 μm and 2.5, respectively. The diagram in the inset of Fig. 5(a) illustrates the second-order WGM field-intensity pattern within the GaN micro-disk at ~438.5 nm ($m = 29$). Regions shaded in red and blue represent the highest and lowest field intensities respectively, while the micro-disk boundary is defined by the black line.

A broadband optical transmission measurement is performed to detect WGMs over wider frequency ranges, using a high-power tungsten-halogen lamp as the incident source. The beam is focused into an optical fiber through a 20× objective lens, which is directed at the micro-disks in proximity using a micro-manipulator. A second fiber probes the transmitted light which is then coupled to an optical spectrometer. Fig. 5(b) shows the measured and normalized transmission spectra from the GaN micro-disk cavity, together with a FDTD-simulated transmission plot. Several transmission minima at specific wavelengths can be observed across the broadband spectra, coinciding well with WGMs predicted through FDTD simulations. The transmission minima are due to coupling of incident light into WGMs within the micro-disk, becoming trapped within the optical cavity. Admittedly, the transmission minima are not as sharp as they should be, limited by the detection fiber probe many times the dimensions of the micro-disks. Consequently, light reflected off the surface of the wafer will diminish the relative strengths of the detected WGM signals.

In summary, the fabrication of high-quality InGaN/GaN micro-disks on Si substrate is demonstrated, employing using microsphere lithography as a patterning technique, followed by dry and wet etching. Optically pumped blue lasing at room temperature has been observed attributed to WGMs. Resonant modes across wide frequency ranges within the micro-disk cavity have been verified by broadband transmission spectroscopy. Numerical calculations and FDTD simulations have also been carried out to determine the mode numbers and pattern of the WGMs in these micro-disk cavities. The work represents a significant step forward towards realizing GaN blue micro-lasers on Si substrates.

This work was supported by a GRF grant of the Research Grant Council of Hong Kong (Project No. HKU 7117/11E).

[1]M. P. Nezhad, A. Simic, O. Bondarenko, B. Slutsky, A. Mizrahi, L. Feng, V. Lomakin, and Y. Fainman, Nat. Photonics **4**, 395 (2010).
[2]L.-M. Chang, C.-H. Hou, Y.-C. Ting, C.-C. Chen, C.-L. Hsu, J.-Y. Chang, C.-C. Lee, G.-T. Chen, and J.-I. Chyi, Appl. Phys. Lett. **89**, 071116 (2006).
[3]S. L. McCall, A. F. J. Levi, R. E. Slusher, S. J. Pearton, and R. A. Logan, Appl. Phys. Lett. **60**, 289 (1992).
[4]J. C. Johnson, H.-J. Choi, K. P. Knutsen, R. D. Schaller, P. D. Yang, and R. J. Saykally, Nature Mater. **1**, 106 (2002).
[5]R. Chen, H. D. Sun, T. Wang, K. N. Hui, and H. W. Choi, Appl. Phys. Lett. **96**, 241101 (2010).
[6]S. Chang, N. B. Rex, R. K. Chang, G. Chong, and L. J. Guido, Appl. Phys. Lett. **75**, 166 (1999).
[7]E. D. Haberer, R. Sharma, C. Meier, A. R. Stonas, S. Nakamura, S. P. DenBaars, and E. L. Hu, Appl. Phys. Lett. **85**, 5179 (2004).
[8]A. C. Tamboli, E. D. Haberer, R. Sharma, K. H. Lee, S. Nakamura, and E. L. Hu, Nat. Photonics **1**, 61 (2007).
[9]I. Aharonovich, A. Woolf, K. J. Russell, T. Zhu, N. Niu, M. J. Kappers, R. A. Oliver, and E. L. Hu, Appl. Phys. Lett. **103**, 021112 (2013).
[10]D. Simeonov, E. Feltin, H.-J. Bühlmann, T. Zhu, A. Castiglia, M. Mosca, J.-F. Carlin, R. Butté, and N. Grandjean, Appl. Phys. Lett. **90**, 061106 (2007).
[11]D. Simeonov, E. Feltin, A. Altoukhov, A. Castiglia, J.-F. Carlin, R. Butté, and N. Grandjean, Appl. Phys. Lett. **92**, 171102 (2008).
[12]H. W. Choi, K. N. Hui, P. T. Lai, P. Chen, X. H. Zhang, S. Tripathy, J. H. Teng, and S. J. Chua, Appl. Phys. Lett. **89**, 211101 (2006).
[13]M. Mexis, S. Sergent, T. Guillet, C. Brimont, T. Bretagnon, B. Gil, F. Semond, M. Leroux, D. Néel, S. David, X. Chécoury, and P. Boucaud, Opt. Lett. **36**, 2203 (2011).
[14]T. Guillet, M. Mexis, S. Sergent, D. Neel, S. Rennesson, C. Brimont, T. Bretagnon, B. Gil, D. Sam-Giao, B. Gayral, F. Semond, M. Leroux, S. David, X. Checoury, and P. Boucaud, Phys. Status Solidi B **249**(3), 449 (2012).
[15]M. Bürger, G. Callsen, T. Kure, A. Hoffmann, A. Pawlis, D. Reuter, and D. J. As, Appl. Phys. Lett. **103**, 021107 (2013).
[16]P. Frajtag, N. A. El-Masry, N. Nepal, and S. M. Bedair, Appl. Phys. Lett. **98**, 023115 (2011).
[17]R. P. Wang and M.-M. Dumitrescu, J. Appl. Phys. **81**, 3391 (1997).